THE MILLI-ARCSECOND STRUCTURE OF A COMPLETE SAMPLE OF RADIO SOURCES. I. VLBI MAPS OF SEVEN SOURCES

T. J. PEARSON AND A. C. S. READHEAD

Owens Valley Radio Observatory, California Institute of Technology Received 1980 November 3; accepted 1981 March 2

ABSTRACT

The sample of 51 sources between declinations 35° and 70° with galactic latitude >10° and flux density \ge 1.3 Jy at 5 GHz contains 36 objects that are suitable for study by very long baseline interferometry (VLBI). Observations have been made of seven of these with a VLBI array of four U.S.A. antennas at a frequency of 5 GHz with full hour-angle coverage. The results show a wide variety of morphologies: two sources (0133+476 and 0859+470) are only slightly resolved, one is a double source (0923+392=4C 39.25) with a constant separation, three (1807+698=3C 371, 1828+487=3C 380, and 2200+420=BL Lac) have an elongated linear structure, and the last (0316+413=3C 84) is complex. Later papers in the series will present the observations of the remaining sources in the sample.

Subject headings: BL Lacertae objects — interferometry — quasars — radio sources: general

I. INTRODUCTION

Recent developments in very long baseline interferometry (VLBI) have made it possible to make aperture synthesis maps of the milli-arcsecond structure of extragalactic radio sources. It is now possible routinely to make reliable observations of high quality at four or more telescopes simultaneously, and the enlargement of the Caltech-JPL Processor to process all 10 baselines from a five-telescope experiment enables us to take full advantage of the extensive (u, v)-plane coverage offered by such observations. The recognition of the value of closure phase (the sum of the visibility phases around a closed loop of baselines: Jennison 1958; Rogers et al. 1974) as a good observable, unaffected by the instrumental and atmospheric instabilities that prevent the measurement of visibility phase, and the development of iterative techniques to estimate the true visibility phases from the measured visibility amplitudes and closure phases (Readhead and Wilkinson 1978; Cotton 1979), have made milli-arcsecond aperture synthesis a reality.

So far this technique has been applied to only a small number of sources. For example, Cohen and his colleagues have mapped the "superluminal" sources 3C 273, 3C 345, and 3C 120, which show apparent expansion velocities greater than the speed of light, at two frequencies and at several epochs (Cohen *et al.* 1979); Readhead and Wilkinson and their colleagues have made low-frequency maps of sources which show synchrotron self-absorption at frequencies below 1 GHz, which may be expected to show structure on angular scales of 0.0.1–0.1 (Wilkinson *et al.* 1977; Wilkinson *et al.* 1979;

Readhead and Wilkinson 1980; Pearson, Readhead, and Wilkinson 1980; Simon et al. 1980). These programs have shown that on the milli-arcsecond scale a large proportion of sources show a characteristic morphology, consisting of a compact, flat-spectrum (presumably selfabsorbed) core, with a steeper-spectrum extension on one side, commonly called a jet. The jet appears to be closely related to the large-scale (arc second) structure of the sources: for example, in the classical double radio galaxy NGC 6251 the milli-arcsecond jet is closely aligned with a much larger-scale jetlike feature which extends out of the galaxy toward one of the two outer lobes (Readhead, Cohen, and Blandford 1977; Cohen and Readhead 1979; see also Linfield 1981). In compact sources without classical double structure, the jet is frequently aligned with such arc-second structure as is present; for example, in 3C 273 the radio jet lies within 30° of the position angle of the optical jet. In these sources, however, the alignment is less perfect than in the classical double sources (Readhead et al. 1978; Readhead 1980). This has suggested that in the compact sources, the jet represents a beam of energy propagating almost directly toward the observer, with its radiation amplified by relativistic aberration (Readhead et al. 1978; Scheuer and Readhead 1979; Blandford and Königl 1979).

It is impossible to assess the statistical significance of these suggestive results without observations of a statistically unbiased sample of sources. Selection on the basis of spectrum, for example, is inadequate as there is known to be a close connection between the angular structure and spectrum of sources. Similarly, to determine how common apparent superluminal expansions are, high-resolution observations are needed of a complete sample at several epochs. The attempts which have been made to determine what fraction of sources show superluminal expansion have suggested that they are quite common, but the estimates are based on very small samples (four superluminal sources in a sample of 10: M. H. Cohen *et al.* 1977).

These are the reasons that led us to make the study of a complete sample of sources that is reported here. This first paper describes the selection of the sample and presents maps of the first seven sources. The maps of the remaining sources, and the discussion of the properties of the sample as a whole, will be the subject of later papers in the series.

II. THE SAMPLE

The choice of a sample for study is governed both by scientific objectives and by observational constraints. To avoid biasing the sample, we chose to select sources by total flux density only. Selection of the sample is thus reduced to three parameters: the frequency of the finding survey, the flux density limit, and the region of sky covered. For the selection frequency we chose 5 GHz, because this is the highest frequency at which full-sky surveys are available, and it is known that the proportion of flat-spectrum, compact objects suitable for study via VLBI increases with selection frequency. 5 GHz is also the frequency of our VLBI mapping observations. The location of suitable telescopes in the northern hemisphere restricts us to northern sources, and in order to achieve the best possible coverage of the (u, v)-plane we further restricted the sample to sources north of declination 35°. The size of the sample is of course restricted by the observing time available and by the sensitivity of the telescopes; it is these constraints that determine the flux density limit.

Our sample is defined by the following criteria:

- 1. Declination: $35^{\circ} < \delta < 70^{\circ}$.
- 2. Galactic latitude: $|b| > 10^{\circ}$.
- 3. Flux density: $S(5 \text{ GHz}) \ge 1.3 \text{ Jy}$.

The sky coverage of the sample is that of the NRAO-MPIfR¹ S4 survey (Pauliny-Toth et al. 1978a) from which the values of S(5 GHz) were taken. The sample so defined contains 51 sources. These sources are listed in Table 1, with their positions, flux densities, optical identifications, and redshifts. The restriction to declinations below 70° was dictated by the absence of a 5 GHz sky survey of higher declinations. With the completion of the MPIfR S5 survey (Kühr et al. 1981) this restriction has been lifted, and we intend to enlarge our sample by removing the northern declination limit.

It is not possible at present to make VLBI maps of all the sources in the sample, because the sensitivity of the VLBI array is insufficient to map sources without a strong compact component. One can decide which sources are mappable on the basis of the observations that have been made with aperture synthesis telescopes, with a resolution of about 1". The sources are classified in Table 1 according to their arc-second-scale morphology.

The extended sources are marked I or II according to their Fanaroff-Riley class (Fanaroff and Riley 1974). The sample includes three of the low-luminosity class I sources (3C 66B, 3C 83.1B=NGC 1265, 3C 449); all of these have compact central components (Preuss et al. 1977; van Breugel et al. 1981), but at ≤100 mJy they are all too weak to be mapped with VLBI. There are 13 high-luminosity class II sources, of which only two (3C 179 and 3C 236) have central components strong enough to map.

There are 34 compact sources ($\lesssim 1''$) in the sample. All of these are candidates for mapping. In Table 1 they are marked U (unresolved), or C ("core"-type: Readhead et al. 1978) if there is low-brightness resolved structure present. Many of the U sources have not yet been studied with sufficient dynamic range at resolutions of $\sim 1''$ to see if they belong in the C class.

The remaining source is 3C 231, associated with the irregular galaxy M82. VLBI observations of 3C 231 have been made by Geldzahler *et al.* (1977) and Shaffer and Marscher (1979). The 5 GHz flux density of the compact component is ~ 150 mJy, which is too weak for mapping, and as it is a completely different sort of object from the others in the sample we shall not consider it further.

These considerations of the arc-second-scale morphology of the sources thus reduce the sample for which VLBI maps are to be made from 51 to 36 sources: 34 compact sources and two extended doubles.

In order to confirm this conclusion, and to avoid wasting valuable observing time on sources that are too weak to map, we conducted a "finding survey" in 1978 July (1978.51), in which we made brief observations of all 51 sources in the sample. An array of four U.S. antennas was used (Table 2), and each source was observed for two periods of 30 minutes each, separated by about 6^h in hour angle. Thus the visibility of each source was measured at 12 points in the (u, v)-plane. (A small number of sources were observed at fewer points, owing to instrumental failures.) Thirty-five of the 36 sources that we expected to detect showed fringes in this survey, the exception being 1634+628 (3C 343). None of the sources that we did not expect to detect showed fringes. As we intended to make maps of the sources, we did not conduct an elaborate analysis of the results of the finding survey, but simply determined the best-fitting circular Gaussian model of each source. The results are

¹National Radio Astronomy Observatory-Max-Planck-Institut für Radioastronomie.

TABLE 1 THE COMPLETE SAMPLE

				S (5GH2	2) Opt		Radio	S(core) size	
Sour (1)	ce (2)	RA (3)	Dec (4)	(Jy) (5)	type m. (6) (7)	(<u>2</u>)	type (9)	(Jy) (10)	(11)	Ref (12)
0040+517 0108+388 0133+476 0220+427 0314+416	3C20 OC314 OC457 3C66B 3C83.1B	00 40 19.70 01 08 47.27 01 33 55.13 02 20 01.73 03 14 56.79	51 47 07.2 38 50 32.6 47 36 13.0 42 45 54.6 41 40 32.6	4.18 1.35 3.26 3.75 3.53	G 19 EF Q 18.0 G 12.9 G 12.5	0.350 (0.86) 0.0215 0.0255	U U I I	<0.01 0.23 0.02	- <1.6 <0.1	JPR,L1 P PW N RP,OBR
0316+413 0538+498 0605+480 0710+439 0711+356	3C84 3C147 3C153 OI417 OI318	03 16 29.56 05 38 43.51 06 05 44.46 07 10 03.33 07 11 05.62	41 19 51.9 49 49 42.8 48 04 49.0 43 54 26.2 35 39 52.6	47.2 8.18 1.35 1.66 1.51	G 11.9 Q 17.8 G 18.5 G 20.7 Q 17.0	0.0177 0.545 0.2769	U C II U U	<0.01	• • • • • • • • • • • • • • • • • • •	ER L2 L1,PH PW PW
0723+679 0804+499 0809+483 0814+425 0831+557	3C179 OJ508 3C196 OJ425 4C55.16	07 23 04.29 08 04 58.40 08 09 59.42 08 14 51.67 08 31 04.37	67 54 52.7 49 59 23.0 48 22 07.2 42 32 07.7 55 44 41.4	1.31 2.07 4.35 1.68 5.60	Q 18.0 Q? 19.0 Q 17.8 Q 17.7 G 17.5	0.846 0.871 0.2420	U U U U	<0.05	-	PW PW PH PW L2
0850+581 0859+470 0906+430 0917+458 0923+392	4C58.17 4C47.29 3C216 3C219 4C39.25	08 50 50.40 08 59 39.97 09 06 17.25 09 17 50.67 09 23 55.31	58 08 55.0 47 02 56.9 43 05 59.4 45 51 43.5 39 15 23.6	1.41 1.78 1.78 2.29 8.90	Q 18.0 Q 18.7 Q 18.5 G 17.2 Q 17.9	1.322 1.462 0.670 0.1744 0.699	n n c	0.04	<0.25	P PFJ JPR B,PBWF ER
0945+408 0951+699 0954+556 0954+658 1003+351	4C40.24 3C231,M82 4C55.17 3C236	09 45 50.04 09 51 41.95 09 54 14.34 09 54 57.83 10 03 05.39	40 53 43.6 69 54 57.5 55 37 16.4 65 48 15.8 35 08 48.0	1.39 3.94 2.27 1.46 1.32	Q 17.5 G 8.4 Q 17.9 Q 16.7 G 16.0	1.252 0.0009 (0.909)	C ? U II	1.50	0.2	PFJ PW P FMB
1031+567 1254+476 1358+624 1409+524 1609+660	OL553 3C280 4C62.22 3C295 3C330	10 31 56.00 12 54 41.05 13 58 58.32 14 09 33.50 16 09 16.16	56 44 18.1 47 36 32.1 62 25 06.7 52 26 13.0 66 04 30.0	1.31 1.53 1.77 6.48 2.35	G 21.3 G 20 G 20.9 G 20.1 G 20.8	0.4614 0.549	U II II II	<0.01 <0.02 <0.02	- -	PW Ll,PH PW Ll,PH JPR,Ll
1624+416 1633+382 1634+628 1637+574 1641+399	4C41.32 4C38.41 3C343 OS562 3C345	16 24 18.22 16 33 30.63 16 34 01.06 16 37 17.43 16 41 17.60	41 41 23.4 38 14 09.9 62 51 41.8 57 26 15.8 39 54 10.8	1.31 4.08 1.50 1.44 10.9	EF Q 18.0 Q 20.6 Q 17.0 Q 16.0	1.814 0.988 0.745 0.595	ນ ດ ດ			PW PW ER P ER
1642+690 1652+398 1739+522 1807+698 1823+568	4C69.21 4C39.49 4C51.37 3C371 4C56.27	16 42 18.03 16 52 11.75 17 39 29.00 18 07 18.54 18 23 14.93	69 02 13.7 39 50 24.6 52 13 10.3 69 48 57.1 56 49 18.1	1.43 1.42 1.99 2.33 1.67	Q 19.2 G 13.8 Q 18.5 G 14.8 Q? 18.9	0.0337 1.375 0.050	ם ס ס			PFJ PFJ PW
1828+487 1842+455 1939+605 1954+513 2021+614	3C380 3C388 3C401 OV591 OW637	18 28 13.54 18 42 35.45 19 39 38.84 19 54 22.46 20 21 13.31	48 42 40.5 45 30 21.6 60 34 32.6 51 23 46.3 61 27 18.1	6.19 1.77 1.52 1.43 2.31	Q 16.8 G 15.3 G 18.0 Q 18.5 SO 19.5	0.692 0.0908 0.201 1.230	C II U U	0.10 0.04	<1.3	L2 PH JPR PW PW
2153+377 2200+420 2229+391 2243+394 2351+456	3C438 OY401 3C449 3C452 4C45.51	21 53 45.49 22 00 39.36 22 29 07.63 22 43 32.81 23 51 49.96	37 46 12.9 42 02 08.6 39 06 03.5 39 25 27.6 45 36 22.9	1.54 4.75 1.39 3.26 1.41	G 19.3 Q 14.5 G 13.2 G 16.0 G? 20.6	0.292 0.069 0.0171 0.0811	II U II U	0.01 0.04 0.13	<0.5 <0.4 <0.8	JPR,L1 ER PWS RP PW
2352+495	OZ488	23 52 37.78	49 33 26.8	1.77	G 19.0	0.2370	ט			ER, FB

EXPLANATION OF TABLE 1

Col. (1).—Source name according to IAU convention.

Col. (2).—Alternative name.

Cols. (3), (4).—Right ascension and declination (1950.0); from Peacock and Wall (1981) when available or from Pauliny-Toth et al. (1978a). All are measured with interferometers and have uncertainties typically less than 0"3.

Col. (5).—Flux density at 5 GHz (Jy), from the S4 survey (Pauliny-Toth et al. 1978a), epoch 1974 December.

TABLE 1-Continued

Col. (6). — Optical identification: EF, Empty field. G, Galaxy. Q, Quasar or BL Lac object. SO, Stellar object.

Col. (7).—Optical magnitude, m_v .

Col. (8). — Redshift. The data in columns (6)–(8) are from the compilations of Burbidge and Crowne (1979), Hewitt and Burbidge (1980), and Peacock and Wall (1981), with the following exceptions: 0040+417 (Laing 1981b), 0108+388 (Johnson 1974), 0954+658 (Walsh, Wills and Wills 1979), 1642+690 (Perley, Fomalont, and Johnston 1980).

Col. (9).—Radio morphology: I, Extended double, Fanaroff-Riley class I. II, Extended double, Fanaroff-Riley class II. C, "Core" source with dominant central component. U, Unresolved by aperture-synthesis telescopes.

Col. (10).—Flux density of central component at 5 GHz (Jy), for class I and class II sources only.

Col. (11).—Angular size of central component (arc seconds), for class I and class II sources only, determined using synthesis telescopes. Col. (12).—References for radio data in columns (9)–(11): B, Burch 1979. ER, Elsmore and Ryle 1976. FMB, Fomalont, Miley, and Bridle 1979. JPR, Jenkins, Pooley, and Riley 1977. L1, Laing 1981b. L2, Laing 1981a. N, Northover 1973. OBR, Owen, Burns, and Rudnick 1978. P, R. A. Perley, private communication. PBWF, Perley et al. 1980. PFJ, Perley, Fomalont, and Johnston 1980. PH, Pooley and Henbest 1974. PW, Peacock and Wall 1981. PWS, Perley, Willis, and Scott 1979. RP, Riley and Pooley 1975.

TABLE 2
THE ANTENNAS

	Location	Diameter (m)	System Temp (K) ^a	Sensitivity (K/Jy) ^b
NRAO	National Radio Astronomy Observatory, Green Bank, West Virginia	43	70	0.31
FDVS	Harvard Radio Astronomy Station, Fort Davis, Texas	26	140	0.082
OVRO	Owens Valley Radio Observatory, Big Pine, California	40	120	0.22
HCRK	University of California, Hat Creek, California	26	70	0.074

^aSystem temperatures are typical values for the run.

^bSensitivities are peak values: there is some variation with the attitude of the antenna.

given in Table 3. Owing to problems calibrating the Fort Davis antenna, we were forced to omit three baselines from this analysis; the fit is thus based on six 30-minute tracks on each source.

Table 3 lists the flux density and diameter (FWHM) of the Gaussian model, obtained by least-squares fit of a straight line of the form

$$\log(S) = a + b(u^2 + v^2),$$

where S is the correlated flux density at the point (u, v). This is the correct statistical procedure to use when the data are affected primarily by multiplicative calibration errors rather than additive noise errors. The linear correlation coefficient r is also listed: a value of -1 indicates perfect correlation, i.e. exact fit to a Gaussian, while positive values of r imply that the visibility increases with increasing baseline, in which case the corresponding diameter is imaginary. The Gaussian parameters should not be taken too literally for sources with r > -0.7.

III. THE FIRST SEVEN SOURCES: OBSERVATIONS AND ANALYSIS

The remainder of this paper is concerned with the observations made in 1978 December of seven sources from the complete sample. The observational technique will be the same for all the sources. In the first observing session we studied seven of the strongest sources: 0133+476, 0316+413, 0859+470, 0923+392, 1807+698, 1828+487, and 2200+420.

The observations, made on 1978 December 11-14 (1978.95), in the frequency band 5.010-5.012 GHz, utilized the same four telescopes as the finding survey (Table 2). This array gives six baselines, ranging in length from 6.2 million to 58 million wavelengths (equatorial component). Hydrogen-maser frequency standards were used at all four stations. The data were recorded on NRAO Mark II terminals (Clark 1973). The feeds were linearly polarized with the *E*-vector in position angle 90° , so the resulting maps represent the distribution of I-Q rather than the total intensity I.

TABLE 3
RESULTS OF THE FINDING SURVEY

Source	Flux Density (Jy)	FWHM (milli-arcsec)	Linear Correlation Coefficient (r)
0108+388	1.14	1.16	-0.63
0133+476	1.77	1.22	-0.93
0316+413	38.3	3.05	-0.73
0538+498	1.52	2.96	-0.89
0710+439	0.79	1.18	-0.47
0711+356	0.96	1.07	-0.58
0723+679	0.31	0.29	-0.04
0804+499	0.49	1.13	-0.77
0814+425	1.60	1.15	-0.87
0831+557	3.23	3.05	-0.99
0850+581	0.88	0.53	-0.32
0859+470	. 0.98	0.83	-0.48
0906+430	0.70		+0.25
0923+392	. 8.89	2.42	-0.90
0945+408	. 1.03	1.21	-0.72
0954+556 ^a		•••	* •••
0954+658	. 0.49	0.39	-0.15
1003+351	. 0.29	1.71	-0.52
1031+567 ^a		• • •	•••
1358+624	. 0.49	1.60	-0.53
1624+416		2.05	-0.75
1633+382	. 1.59	1.35	-0.88
1634+628 ^b		•••	• • • •
1637+574	. 0.81	• • •	+0.20
1641+399		1.50	-0.43
1642+690			+0.13
1652+398	. 0.65	1.19	-0.82
1739+522	. 0.39	0.56	-0.10
1807+698	. 1.21	1.40	-0.58
1823+568		• • •	+0.19
1828+487			+0.52
1954+513		0.97	-0.26
2021+614		1.70	-0.48
2200+420		1.77	-0.69
2351+456	. 0.95	2.09	-0.96
2352+495	. 1.62	1.00	-0.96

^aLess than 3 (u, v) points detected: these sources are heavily resolved.

The data were cross-correlated using the Caltech/JPL Interferometry Processor. The processor output was integrated coherently for 120 s. The visibility amplitudes were calibrated in the usual way (Cohen et al. 1975) and used with the closure phase to make hybrid maps by the method of Readhead and Wilkinson (1978). The calibrated visibility amplitudes and closure phases are presented in the Appendix.

The accuracy of the maps depends on the (u, v)coverage, sensitivity, and dynamic range of the observations.

a) (u, v)-Coverage

As far as possible, each source was observed continuously for the full period for which it was visible from all four telescopes, generally between 9.5 and 11.5 hours;

0133+476 was observed for only 5 hours and 1807+698 for 8 hours. A typical example of the (u, v)-coverage obtained is shown in Figure 1. While this coverage is good by comparison with what has been available in past VLBI experiments, it does not approach the completeness of coverage achieved with purpose-built aperture synthesis instruments. In the absence of any a priori information about the source, the sampling theorem tells us that to map a source of size less than θ with resolution $\delta\theta$, we need to sample the (u, v)-plane every $1/\theta$ wavelengths out to a maximum of $1/\delta\theta$ wavelengths. This sampling requirement on the uniformity of the (u, v)-coverage is not satisfied in the present observations, and we must therefore remember that there may be real features of the source which are not represented or are incorrectly represented in the maps. Blind tests, like those conducted by Readhead and Wilkinson (1978), give us some confidence that the (u, v)-coverage is adequate to map simple sources, but of course we do not know a priori that the sources are sufficiently simple. The sampling requirement is unlikely to be satisfied with any array of presently existing telescopes, and fully reliable VLBI maps must await the construction of a carefully designed VLBI array.

b) Sensitivity

In the present observations the coherent integration time was 120 s and the bandwidth was 2 MHz; the system temperatures and sensitivities of the antennas are given in Table 2. From these data one can calculate the rms noise in a single integration, following the procedure described by Cohen *et al.* (1975): the noise varied from 0.14 Jy on the least sensitive baseline (FDVS–HCRK) to 0.04 Jy on the best baseline (NRAO–OVRO).

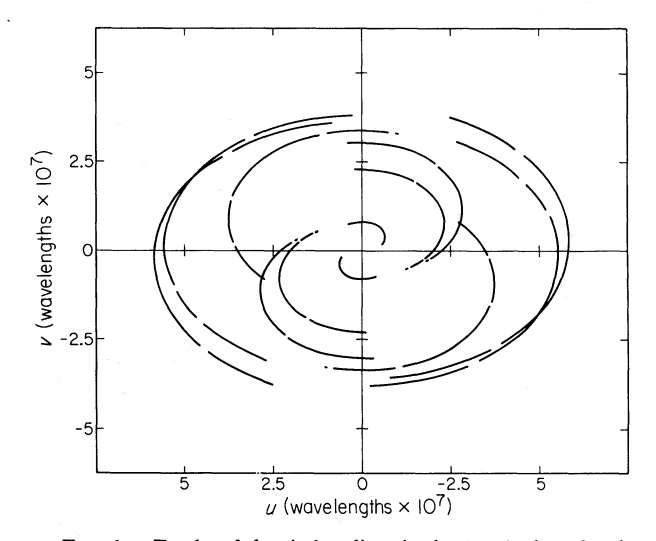


FIG. 1.—Tracks of the six baselines in the (u, v)-plane for the observation of 3C 84 (0316+413). The conjugate tracks are also shown. Occasional gaps are due to tape changes.

^bNot detected in the finding survey.

The correlated flux density should be at least 3 times the noise level for a reliable detection. The system noise gives rise to errors in the map, but these errors are always much smaller than the errors due to poor dynamic range (Readhead et al. 1979).

c) Dynamic Range

The dynamic range (the ratio of the strongest feature to the weakest believable feature) of the maps is limited by the gaps in the (u, v)-coverage and by uncertainties in the calibration. The relative scaling of the different baselines is uncertain by about 5%. From experiments with simulated observations (cf. Readhead and Wilkinson 1978) and by comparing the results of real observations with four and five stations, we have found that the dynamic range of the maps is usually about 20:1. This means that contours at 5% and below in the maps presented in the figures are unreliable.

IV. DISCUSSION OF INDIVIDUAL SOURCES

The seven sources observed are listed in Table 4. which gives the total flux density of each source at the epoch of observation, the effective resolution, and the linear scale of each map. The effective resolution is specified by the parameters of the restoring beam used in the hybrid mapping. The restoring beam is an elliptical Gaussian with FWHM chosen to match as closely as possible the FWHM of the "dirty beam" produced by the Fourier inversion. Use of a smaller restoring beam is dangerous, in that it can produce a map with incorrect features. The linear scale of the maps (in parsecs per milli-arcsecond) was calculated assuming a Hubble constant $H_0 = 55 \text{ km s}^{-1} \text{ Mpc}^{-1}$ and deceleration parameter $q_0 = 0.05$; these values were used for all the linear dimensions quoted in this paper. Spectral index is defined by $S \propto v^{\alpha}$.

a) 0133+476 (OC 457, DA 55)

The radio source 0133+476 is compact and has an unusually flat radio spectrum. It has been identified with an 18-mag blue stellar object (A. M. Cohen et al. 1977). The optical spectrum of this object has been observed by Strittmatter et al. (1974), who found only one possible emission line, at 520 nm; it is therefore generally described as a BL Lacertae object. A redshift of 0.86 has been quoted in the literature (Medd et al. 1972; Hewitt and Burbidge 1980), but it is not clear on what evidence this is based. 0133+476 is a strongly variable source: Andrew et al. (1978) measured its flux density at 10.7 GHz and 6.7 GHz between 1966 and 1976, in which period its flux density varied between 2 and 6 Jy; in recent years its 5 GHz flux density has been decreasing, from 3.26 Jy (S4 survey, 1974 December), through 2 Jy (Weiler and Johnston 1980, 1978 March-June) to 1.8 Jy at the epoch of our observations (1978 December). VLBI observations have been made at 5 GHz by Weiler and Johnston (1980), who included it in their study of BL Lacertae objects, and at 1.67 GHz and 10.7 GHz by Marscher and Shaffer (1980).

Owing to the constraint of the observing schedule, we observed 0133+476 for only 5 hours, but the structure of the source appears to be sufficiently simple that this is not a serious limitation. The closure phases do not depart from zero by more than 15°, and the correlated flux densities range between 1.8 Jy on the shortest baseline and 1.2 Jy on the longest baseline. This behavior indicates that the source is only slightly resolved. It is conventional in such cases to model the brightness distribution as an elliptical Gaussian. The best-fitting Gaussian model has a total flux density of 1.7 Jy and axes (FWHM) 1.5 and 1.0 milli-arcsec, with the longer axis in position angle 144°. This implies that the maximum brightness temperature is greater than 55 GK (1 $GK = 10^9$ kelvin). The 5 GHz observations of Weiler and Johnston were made with a longer baseline (Germany-West Virginia) than those used here, and with very restricted (u, v)-coverage, but they found a position angle of 140°, in excellent agreement with our 144°. The equivalent Gaussian diameter (0.7 milli-arcsec) is smaller than ours, perhaps indicating the presence of an unresolved core.

TABLE 4 THE FIRST SEVEN SOURCES

	TOTAL FLUX	Effective Resolution ^a			REDSHIFT	Scale ^b	
Source	DENSITY (Jy)	Major	Minor	PA (°)	- Z	(pc/milli-arcsec)	
0133+476	1.8	4.0	1.8	-18	0.86?	9.2	
0316+413	57.0	2.8	2.2	+11	0.0177	0.46	
0859+470	1.7	2.9	2.1	+11	1.462	10.5	
0923+392	7.5	3.0	2.2	+15	0.699	8.5	
1807+698	2.4	2.8	1.7	-10	0.05	1.2	
1828+487	3.0	2.9	2.1	+10	0.692	8.4	
2200+420	2.3	2.9	2.4	+11	0.069	1.7	

 $^{^{\}rm a}$ FWHM of the Gaussian restoring beam (milli-arcsec). $^{\rm b}H_0$ = 55 km s $^{-1}$ Mpc $^{-1},~q_0$ = 0.05.

TABLE 5
GAUSSIAN MODELS

			FLUX DENSITY	DISPLACEMENT FROM A		Major Axis	AXIAL	PA of Major
Source	Component		(Jy)	(mas)	in PA(°)	FWHM (mas)	Ratio	Axis (°)
0133+476	A	1.67 GHz ^a	2.06			5.1	0.42	170
	Α	5 GHz	1.7			1.5	0.63	144
	Α	10.7 GHz ^a	2.6			0.82	0.53	125
0859+470	A		1.15			2.1	0.43	0
0923+392	A		4.65			1.1	1	
	В		2.34	1.89	-83	0.30	1	
2200+420	A		1.19			0.53	1	
	В		0.65	3.0	183	1.6	1	
	C		0.15	6.7	174	3.0	1 -	

^a Marscher and Shaffer 1980.

Table 5 compares our 5-GHz model with the 10.7 GHz and 1.67 GHz models (derived from observations made about a year before ours) of Marscher and Shaffer (1980). It is clear that the position angle rotates as the frequency increases and the angular scale decreases. This behavior has been observed in other sources by Readhead et al. (1978), but in the present case it is particularly marked. The new 5 GHz observations also confirm the observation of Marscher and Shaffer that the effective angular size of the source increases linearly with wavelength. The spectrum of 0133+476 was measured at epoch 1978.0 by Owen, Spangler, and Cotton (1980): its flux density was almost constant at 2.15 Jy throughout the observed frequency range (750 MHz to 90 GHz). Marscher and Shaffer show that this flat spectrum and the linear increase of size with wavelength can be interpreted most simply in terms of a single, inhomogeneous synchrotron component (Marscher 1977).

It would be of great value to have measurements of the spectrum of 0133+476 at several epochs, to determine whether the decrease in flux density during 1978 that was observed at 5 GHz occurred throughout the spectrum. Further VLBI observations of the source are also required to determine how the structure of the source varies while the total flux density changes.

b) 0316+413 (3C 84, NGC 1275)

The radio source 3C 84 is the strongest in our sample. It has received considerable attention from VLBI observers because of its intensity and variability. It has been studied particularly well at 2.8 cm (10.6 GHz) (Pauliny-Toth et al. 1976; Preuss et al. 1979) and 1.35 cm (22 GHz) (Pauliny-Toth et al. 1978b; Matveenko et al. 1980); the papers cited give full references to earlier observations: The majority of these observations have measured amplitude only. At lower frequencies, a hybrid map based on amplitude and closure phase has been made by Wilkinson et al. (1979) at 50 cm (609)

MHz). This map (of necessity) has a much lower resolution (FWHM 10 milli-arcsec) than the higher-frequency observations.

Our 6 cm (5 GHz) map, with a resolution (FWHM) of about 2.5 milli-arcsec, is shown in Figure 2, and the delta-function model that this map represents is compared with the measured data in the Appendix (Fig. 9). Comparison of this map with published maps at higher and lower frequencies is difficult owing to the varying resolution of the observations, and because the structure of 3C 84 is highly frequency-dependent, with several centers of high-frequency emission embedded in a larger, steeper-spectrum halo ~20 milli-arcsec (9 pc) across. The galaxy also exhibits radio emission on scales of 30" and $\sim 5'$. A full discussion of the 5 GHz map and a comparison with data from other epochs and at different frequencies is deferred to a separate paper. It is clear, however, that the radio structure of 3C 84 is markedly different from the structure of any other object mapped with VLBI. The majority of these objects show a linear structure, consisting either of a core with a one-sided jet, or of two roughly equal components, sometimes connected by a bridge of emission. The radio source 3C 84 does not have a linear structure, and it shows no evidence of the collimation required to produce the core-jet morphology.

The associated optical galaxy, NGC 1275, is also an unusual object. Its optical classification is subject to uncertainty: it is generally called a Seyfert galaxy, but there is no evidence for spiral structure; it is sometimes classified as an elliptical, although the Balmer absorption-line spectrum suggests that the stellar population is younger than that of a typical elliptical galaxy. The main emission-line system is at 5300 km s⁻¹, but there is filamentary structure on one side of the nucleus at 8300 km s⁻¹. These two systems were identified by Minkowski (1957), who suggested that they are two colliding galaxies—a hypothesis which might explain the unusual radio structure. In a detailed discussion of more recent optical and radio observations, however,

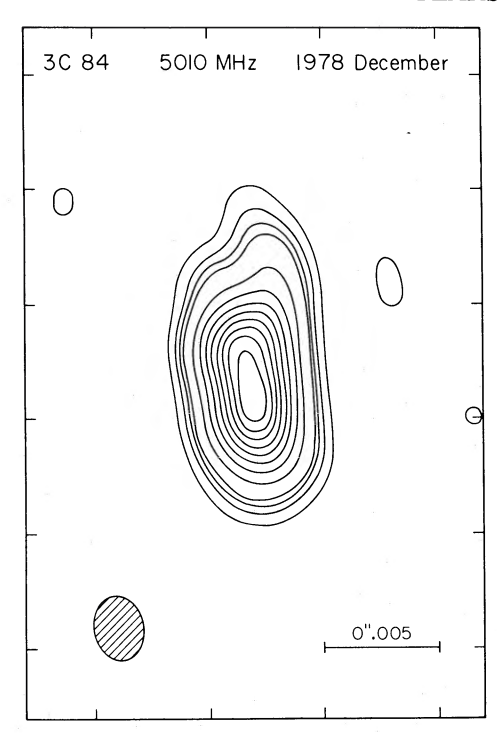


FIG. 2.—Hybrid map of 3C 84 (0316+413). The contour levels are 2.5, 5, 7.5, 10, 20, 30, 40, 50, 60, 70, 80, and 90% of the maximum, which has a brightness temperature of 120 GK. There are no negative contours at -2.5% or below. The hatched ellipse shows the half-power contour of the restoring beam. The frame is marked at intervals of 5 milli-arcsec. In this figure and the other maps (Figs. 3, 4 and 5) north is up and east to the left.

Kent and Sargent (1979) have shown that the 8300 km s⁻¹ system is probably an unrelated spiral galaxy seen in projection against NGC 1275.

c) 0859+470 (4C 47.29, OJ 499)

The radio source 0859+470 is identified with a 19-mag quasar with a redshift of 1.462 (Carswell and Walsh, quoted by Hewitt and Burbidge 1980). A 5 GHz map from the VLA published by Perley, Fomalont, and Johnston (1980) shows that the source consists of a core emitting about 90% of the flux density, an extension 2" to the north, and a possible extension 1" to the southeast.

Our VLBI data show no large variations in visibility, and the closure phases do not depart significantly from zero. The data can be closely reproduced by the elliptical-Gaussian model shown in Table 5. This model accounts for only 70% of the total flux density of the source measured at the same epoch, so the remaining 30% must be attributed to extended components. The hybrid map is essentially identical to this Gaussian model, so we do not present it here.

d) 0923+392 (4C 39.25, DA 267)

The radio source 0923+392 is an 18-mag quasar with a redshift of 0.699. It has been observed many times in VLBI experiments (e.g., Shaffer *et al.* 1977; Bååth *et al.* 1980) and has always appeared to consist of two components. Although the strengths of the two components have varied, their separation has remained fixed at about 2 milli-arcsec (55 lt-yr).

Our observations can be closely reproduced by a model consisting of two circular Gaussian components (Table 5). The hybrid mapping procedure produces a delta-function model that fits the data slightly better than the two-component model but is otherwise indistinguishable. In the map itself the double structure is not clearly apparent, owing to the convolution with the restoring beam, so we do not present it here. The angular separation of the two components is determined fairly precisely by the location of the minima in the visibility function, but the other parameters of the deconvolution are less certain. It is difficult to estimate the uncertainty in the measured separation owing to the possible presence of systematic errors, but the error is certainly not greater than 0.1 milli-arcsec.

The model of Table 5 can be directly compared only with other observations at 5 GHz, of which there have been very few. In 1974.05 the components had flux densities 6.9 Jy and 1.6 Jy and separation 2.02 milliarcsec in position angle 96° (or -84°) (Pauliny-Toth et al., quoted by Shaffer et al. 1977). Thus between 1974.05 and 1978.95 the position angle has remained constant, the separation has, if anything, decreased, and the flux densities of both components have changed. It is reasonable to assume that the stronger component of 1974.05 is still the stronger component, although this cannot be proved because no phase measurements were made in 1974.05; if this is the case, the stronger component, A, has weakened and component B has strengthened since 1974.

More observations are available at higher frequencies. Bååth et al. (1980) report 7.85 GHz observations for 16 epochs between 1972.3 and 1975.1, with varying quality of (u, v)-coverage, and Shaffer et al. (1977) report observations at 10.7 GHz and 14.8 GHz between 1972.3 and 1974.5. In all cases the separation was 2.0 milliarcsec, with a maximum possible error of 0.1 milliarcsec. The apparent decrease in separation between 1972.3 and 1978.9 is thus 0.1 ± 0.1 milliarcsec, corresponding to a velocity of $(0.4\pm0.4)c$.

Both Shaffer et al. and Bååth et al. have attempted to analyse the spectrum of 0923+392 in terms of three homogeneous, self-absorbed synchrotron components and a transparent steep-spectrum component. Two of these components correspond to the VLBI components A and B. The changes in 5 GHz flux density of A and B since 1974.05 appear to be consistent with the evolution-

ary scheme postulated by Shaffer et al., but observations at a higher frequency would be helpful to confirm this.

The steep-spectrum component has been detected by Perley and Johnston (1979) using the Very Large Array (VLA) at 1400 MHz. It has the appearance of a halo or asymmetric double with a position angle of $30^{\circ} \pm 10^{\circ}$, which is apparently unrelated to the VLBI position angle. An unpublished 5 GHz VLA map by Perley shows two secondary components ≈ 1.75 away from the nucleus in position angles 80° and -120° ; again the relationship between this structure and the milliarcsecond double is unclear.

e) 1807+698 (3C 371)

The radio source 3C 371 is identified with a 14–15 mag N galaxy in a small cluster (Sandage 1966). The spectrum of this object has weak emission lines with a redshift of 0.05, the stellar absorption lines normally seen in E galaxies, and a highly variable nonthermal continuum (Miller 1975), which has led to comparisons with BL Lacertae objects (Miller 1975; Miller, French, and Hawley 1978).

The arc-second-scale radio structure of 3C 371 has recently been studied by Perley and Johnston (1979) and by Perley, Fomalont, and Johnston (1980), using the VLA. It is an asymmetric, D2 (Miley 1971) object with a strong, flat-spectrum core, and a weaker, steep-spectrum component extending away from the core on one side, in position angle -115°. There is also a low-brightness "halo."

The hybrid map of the flat-spectrum core, derived from our VLBI observations, is shown in Figure 3. The structure is linear, consisting of a strong component with a maximum brightness temperature in excess of 9 GK, a secondary component 4.5 milli-arcsec (18 lt-yr) away in position angle -97° , and an extension from the

strong component toward the weaker one. Both the secondary component and the extension define the same position angle, which is remarkably close to the position angle of component A on the 5 GHz VLA map (Perley, Fomalont, and Johnston 1980), -115°. The difference of 8° is significant, however. Thus 3C 371 appears to resemble other D2 sources, such as 3C 273 and 3C 345, in showing a one-sided "jet" directed approximately, but not exactly, toward the outer arc-second-scale structure. Unfortunately the dynamic range of the present observations does not permit us to determine whether the structure is really a continuous "jet," or how far it extends from the strong component. Further VLBI observations at other frequencies are needed to determine the spectra of the various components; there is also a prospect of measuring an expansion velocity, but this may be difficult because the visibility does not show sharp minima like those that have been used to trace the superluminal expansion of 3C 273 and 3C 345.

A number of previous VLBI detections of 3C 371 have been reported (Wittels *et al.* 1978 and references therein; Shaffer 1978), but they are all measurements of visibility at a single point in the (u, v)-plane and cannot be compared with the present observations because of the variations in the source.

The spectrum of 3C 371 for 1978.0 (Owen, Spangler, and Cotton 1980) is fairly flat and smooth between 1 GHz and 90 GHz, which would be more consistent with the inhomogeneous synchrotron models of Marscher (1977) than with a model consisting of a small number of discrete, homogeneous components.

The radio source 3C 380 is a 17-mag quasar with a redshift of 0.692. Observations with the Cambridge 5 km telescope (Laing 1981a) and with the VLA

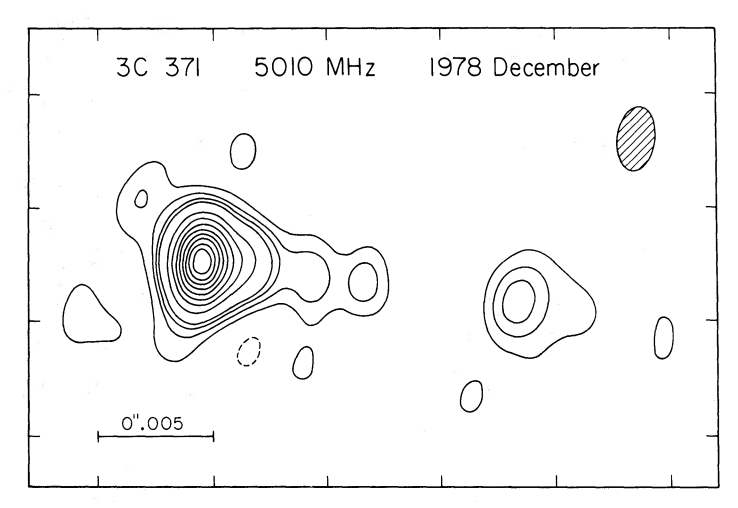


Fig. 3.—Hybrid map of 3C 371 (1807+698). The contour levels are -2.5 (dashed), 2.5, 5, 7.5, 10, 20, 30, 40, 50, 60, 70, 80, and 90% of the maximum, which has a brightness temperature of 9.4 GK. The hatched ellipse shows the half-power contour of the restoring beam. The frame is marked at intervals of 5 milli-arcsec.

PEARSON AND READHEAD

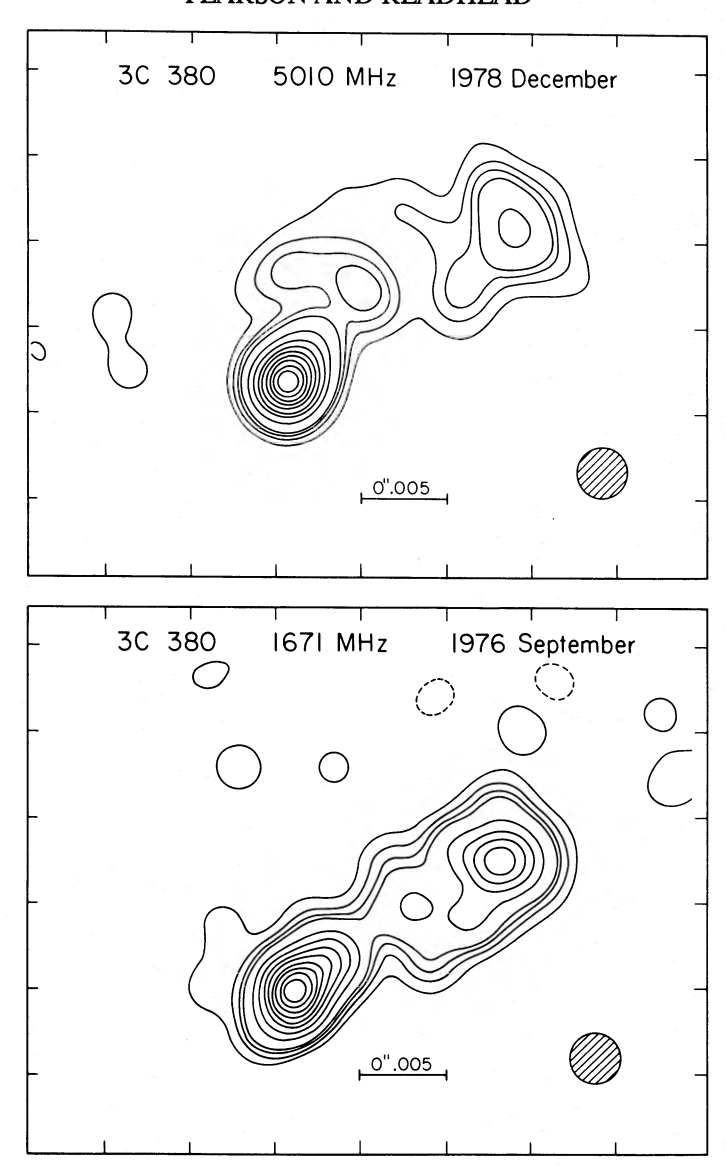


FIG. 4.—Hybrid maps of 3C 380 (1828+487). The 5010 MHz map (top) is from the present work; the 1671 MHz map (bottom) has been redrawn from the data of Readhead and Wilkinson (1980). The same restoring beam, a circular Gaussian of FWHM 3 milli-arcsec, has been used for both maps (hatched ellipse). The contour levels are -2.5 (dashed), 2.5, 5, 7.5, 10, 20, 30, 40, 50, 60, 70, 80, and 90% of the maximum, which has a brightness temperature of 5.7 GK at 5010 MHz and 46 GK at 1671 MHz. The frame is marked at intervals of 5 milli-arcsec.

(Wilkinson et al. 1981) have shown that it has a strong, compact central component with a jetlike structure extending to a distance of about 1".5 from the nucleus in position angle -47° . There is also a steeper-spectrum halo extending about 3" on both sides of the nucleus. A VLBI map of 3C 380 with a resolution of 3 milli-arcsec (FWHM) has been made by Readhead and Wilkinson (1980) at a frequency of 1671 MHz; this map can be directly compared with the new 5 GHz map derived from observations made 2.2 yr later. Both maps are shown in Figure 4; to facilitate the comparison, the same restoring beam has been used for both maps.

The 5 GHz observations had less complete (u, v)-coverage than the 1671 MHz observations, so the dynamic range is slightly worse; and even on the shortest baseline the source is strongly resolved, so large-scale structure is poorly represented in the map. The two maps are remarkably similar, however: both show a strong component A to the southeast and a weaker, more diffuse component B to the northwest, and in both maps the position angle of the line joining the components is -57° . The separation of A and B is different, though: 14 milli-arcsec at 1671 MHz and 16 milli-arcsec at 5 GHz (about 400 lt-yr). In both maps A is more

resolved on the northwest side than on the southeast side. The low-brightness structure between the two components is less constrained by the data, and it is not clear to what extent the differences should be considered significant. The distant component detected at 1671 MHz, 0".73 from the nucleus, was not and could not have been detected in the 5 GHz observations owing to the lack of short baselines.

Figure 5 shows profiles of the brightness temperature along the axis of the source at the two frequencies. The two profiles have been aligned so that the peak and southeast edge of component A coincide at the two frequencies. This is the most plausible alignment, but the correct way to align the profiles is unknown because of the lack of absolute phase measurements. A shift of one profile relative to the other of more than 2 milliarcsec can be ruled out because it would give component A an implausible spectrum.

If component A is aligned as in Figure 5, however, the peak of component B does not coincide at the two frequencies; B must have an inverted spectrum ($\alpha \approx 0.6$) on its "leading" (northwest) edge and a steep spectrum ($\alpha \approx -1.0$) on its trailing edge. In this respect it resembles the knots in the jet of 3C 147 (Readhead and Wilkinson 1978).

An alternative but less plausible alignment would be for the peak of component B to coincide at the two frequencies. This is just permitted by the constraints discussed above. In this case B has a spectral index of -0.7, while A has a steeply rising spectrum on the

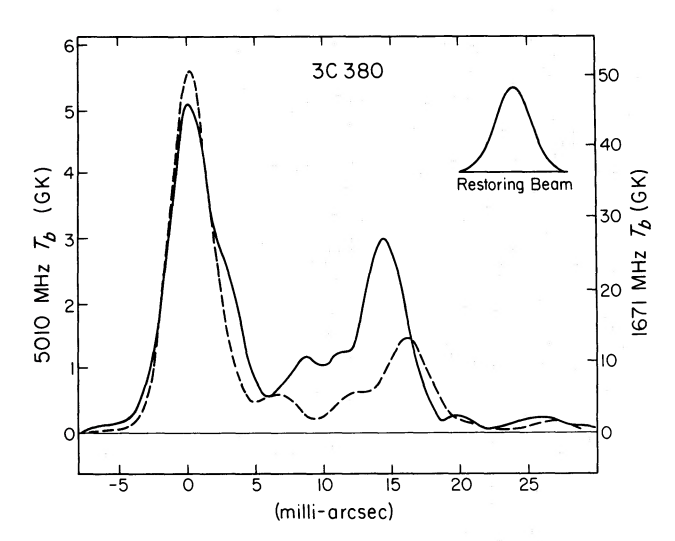


FIG. 5.—Profiles of brightness temperature T_b along the axis of 3C 380 (position angle -57°) at 5010 MHz (dashed line) and 1671 MHz (full line). The brightness temperature scales (left: 5010 MHz; right: 1671 MHz) have been chosen so that an unresolved point source with a flat spectrum (α =0) would give equal deflections at both frequencies. Where the dashed line lies above the full line, α >0 (inverted spectrum); where the dashed line lies below the full line, α <0. Spectral index is defined by $S \propto \nu^{\alpha}$. The profile of the restoring beam (FWHM=3 milli-arcsec) is indicated.

southeast side and a steeply falling spectrum on the northwest side.

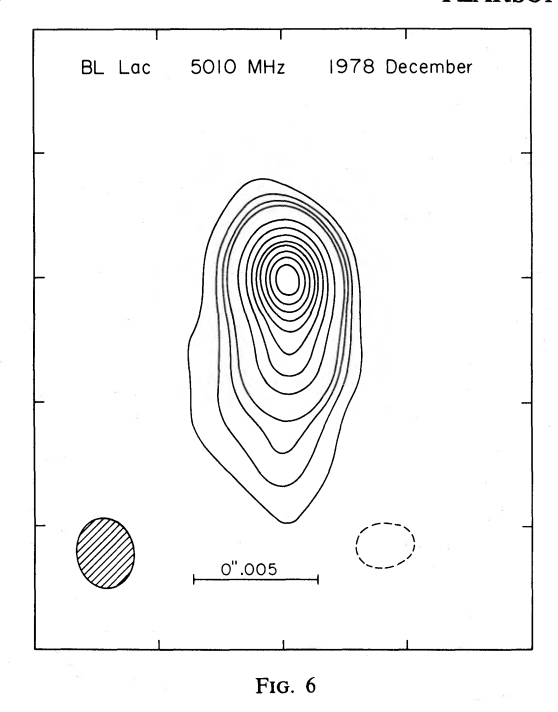
There is another problem in comparing the two profiles, in that the effects of spectrum cannot be distinguished from variations in structure between the 1974.7 (1671 MHz) and 1976.9 (5 GHz) observations. For example, it is possible that the separation has increased due to the motion of one of the components: the apparent velocity would be \sim 0.8 milli-arcsec per year, or about 40 c. Further observations are required to rule out structural changes.

The maps of 3C 380 can be interpreted most simply in terms of the "core-jet" picture of compact sources (Readhead et al. 1978). Component A is the core, with a flat spectrum indicative of synchrotron self-absorption, and the jet extends toward component B in about the same position angle as the arc-second scale jet seen in the Cambridge and VLA maps. Component B is a "knot" in the jet. Readhead and Wilkinson (1980) discussed two alternative origins for the knot: a shock wave in the jet (Rees 1978) and an interaction between the jet and interstellar matter (Blandford and Königl 1979). The fact that the knot has a flatter spectrum on its outer edge, which is sharper than the trailing edge, perhaps favors the first alternative.

g) 2200+420 (BL Lacertae)

BL Lacertae has received considerable attention from VLBI observers; the observations up to the end of 1977 have been summarized by Shaffer (1978). Kellermann et al. (1977) made observations on six baselines at 10.6 GHz and one baseline at 15 GHz and found the radio source to be elongated in position angle 10°. They interpreted the data in terms of a two-component model with separation 1.25 milli-arcsec. Comparison with earlier observations showed that in spite of the large changes in the total flux density, the position angle had remained nearly constant over a period of four years. The separation of the components had apparently varied, but the detailed behavior is unclear owing to the ambiguities of model-fitting with limited (u, v)-coverage. More recent observations of BL Lacertae at 5 GHz (epoch 1979.2, Bååth et al. 1981) continue to show a north-south elongation.

Our 5 GHz map of BL Lacertae is shown in Figure 6. It too has a predominant position angle close to zero. The resolution of this map is about a factor of 4 worse than the observations of Kellermann et al. made in 1974.5. The map appears to show continuous emission along a trail extending about 7 milli-arcsec (40 lt-yr) south from the brightest point. The profile of brightness temperature along a north-south line (Fig. 7) shows two clear shoulders, indicating that the source consists of at least three distinguishable components. In order to make this deconvolution more quantitative, we derived a three-component model by least-squares fitting to the



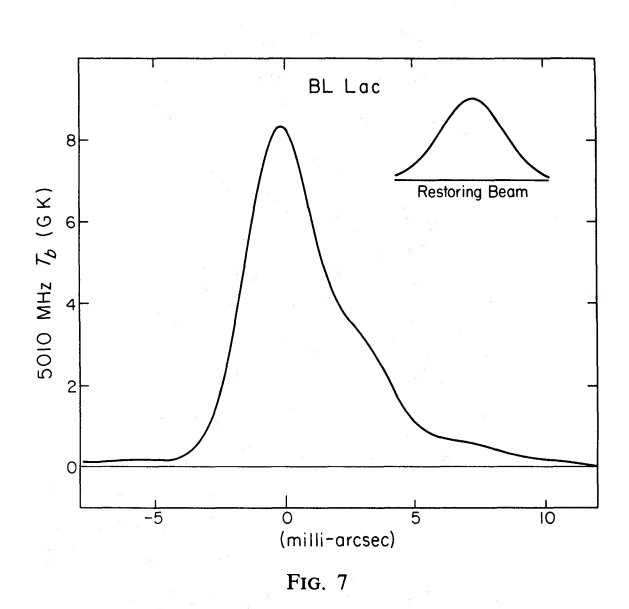


FIG. 6.—Hybrid map of BL Lac (2200+420). The contour levels are -2.5, 2.5, 5, 7.5, 10, 20, 30, 40, 50, 60, 70, 80, and 90% of the maximum, which has a brightness temperature of 8.3 GK. The hatched ellipse shows the half-power contour of the restoring beam. The frame is marked at intervals of 5 milli-arcsec.

Fig. 7.—Profile of brightness temperature T_b along a north-south line through the peak of emission from BL Lac. The profile of the restoring beam is indicated.

visibility amplitudes (Table 5). The fit of this model to both the amplitudes and closure phases is virtually indistinguishable from the fit of the hybrid map.

It should be remembered that this model is a deconvolution, and therefore subject to some uncertainty, but it is suggestive: the components lie almost on a straight line with a position angle that has remained more or less constant for several years, and the progression from A to B to C is one of both decreasing flux density and increasing size. It would be attractive to identify each component with a single expanding synchrotron cloud, with A being the youngest and B and C relics of earlier outbursts, which have moved away from their origin at A along a channel which is preserved between outbursts. If A, B, and C represent successive outbursts separated by less than a year, then apparent velocities considerably in excess of c would be involved. At present, this picture must be regarded as speculation, but it can be confirmed or disproved by regular VLBI monitoring of BL Lacertae at a single frequency (or, preferably, two frequencies) at intervals comparable with the time scale of the total flux density variations, that is, a few months. The observations presented here were made while the flux density was unusually low, and it has since increased by more than a factor of 4. It is particularly important to find out whether the rapid flux density variations affect the whole source or only one component.

V. DISCUSSION

It would be premature to attempt to draw general, quantitative conclusions from the observations presented here, which refer to a nonrandom subset of seven sources from the complete sample. These seven should be representative of the strongest sources in the sample, however.

The source 3C 84 is (at present) the most intense in the sample, and also one of the closest. It is a very peculiar object in both its optical and its radio properties, and is apparently far from being a typical source.

Among the other sources the "core-jet" morphology occurs in at least two of the seven sources, 3C 371 and 3C 380, and perhaps in a third, BL Lacertae. To these we can add 3C 345, which is the second most intense source in the sample. We did not observe 3C 345 because it has already been well studied, and maps have been made at several epochs (Readhead *et al.* 1979; Cohen *et al.* 1981). In spite of their similar radio morphology, however, these four sources are a very mixed bunch; two are quasars with redshifts 0.595 (3C 345) and 0.692 (3C 380), one is a low-redshift BL Lac object (BL Lacertae), and one is a low-redshift N galaxy (3C 371).

The source 0923+392 (4C 39.25) is the third most intense in the sample and, as a compact double source, appears to represent a second morphology. Whether this

is common morphology remains to be seen, and we cannot yet say whether the distinction between such sources and the core-jet sources is not an artificial one due to inadequate dynamic range.

The remaining two sources (0133+476, 0859+470) were only partially resolved in our observations, with angular sizes ≤2 milli-arcsec. Intercontinental baselines and higher frequencies are needed to resolve such sources.

The observations described here were made under the auspices of the U.S.A. VLBI Network Users Group. We thank the many people involved in scheduling the

observations, recording the data at the participating observatories, and processing the tapes, for their indispensable contributions to this paper. We also thank R. A. Laing, J. A. Peacock, and R. A. Perley for communicating results in advance of publication, and the referee for his helpful comments. The work was supported by the National Science Foundation via grants AST 77-00247 and AST 79-13249 to the Owens Valley Radio Observatory; the National Radio Astronomy Observatory is operated by Associated Universities, Inc., under contract with the NSF; astronomical VLBI at Harvard Radio Astronomy Station and Hat Creek Radio Astronomy Observatory is supported by the NSF.

APPENDIX

Figures 8–14 reproduce the measured visibility amplitudes on each of the six interferometer baselines and the closure phases for each of the four baseline triangles; only three of these four closure phases are independent. The measurements are represented by 2σ error bars. The curves superposed on the data points are derived from either Gaussian models or the hybrid maps, as indicated in the figure legends. In the case of the hybrid maps, the curves are derived from the delta-function models (not convolved with the restoring beam). In most cases the hybrid maps reproduce the data exactly. The worst discrepancies occur in the closure phase for 3C 84—the closure phase errors are worst where the amplitudes are small, and can be attributed to the limited dynamic range.

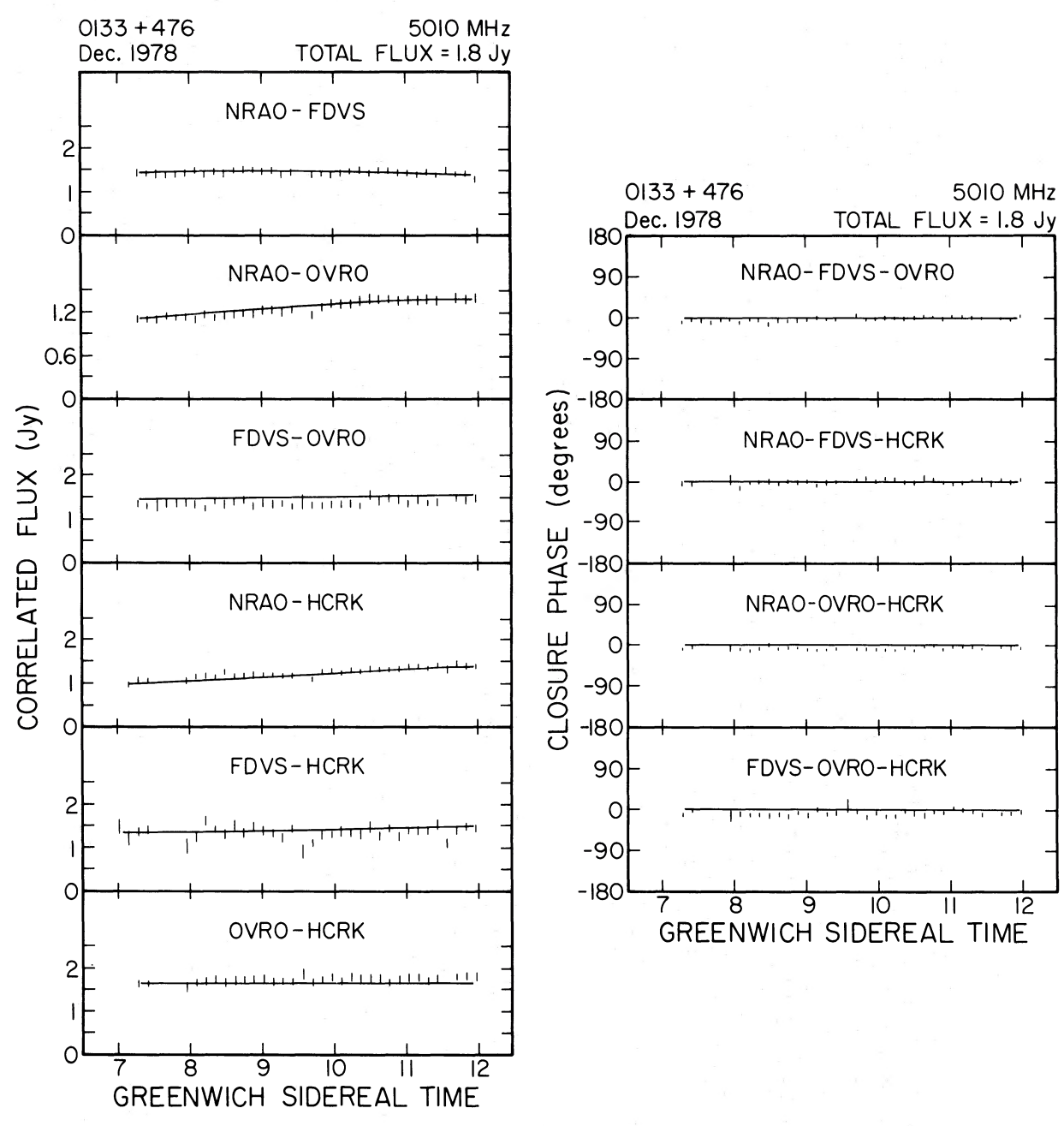


Fig. 8.—Visibility amplitudes and closure phases for 0133+476. The model is an elliptical Gaussian (Table 5).

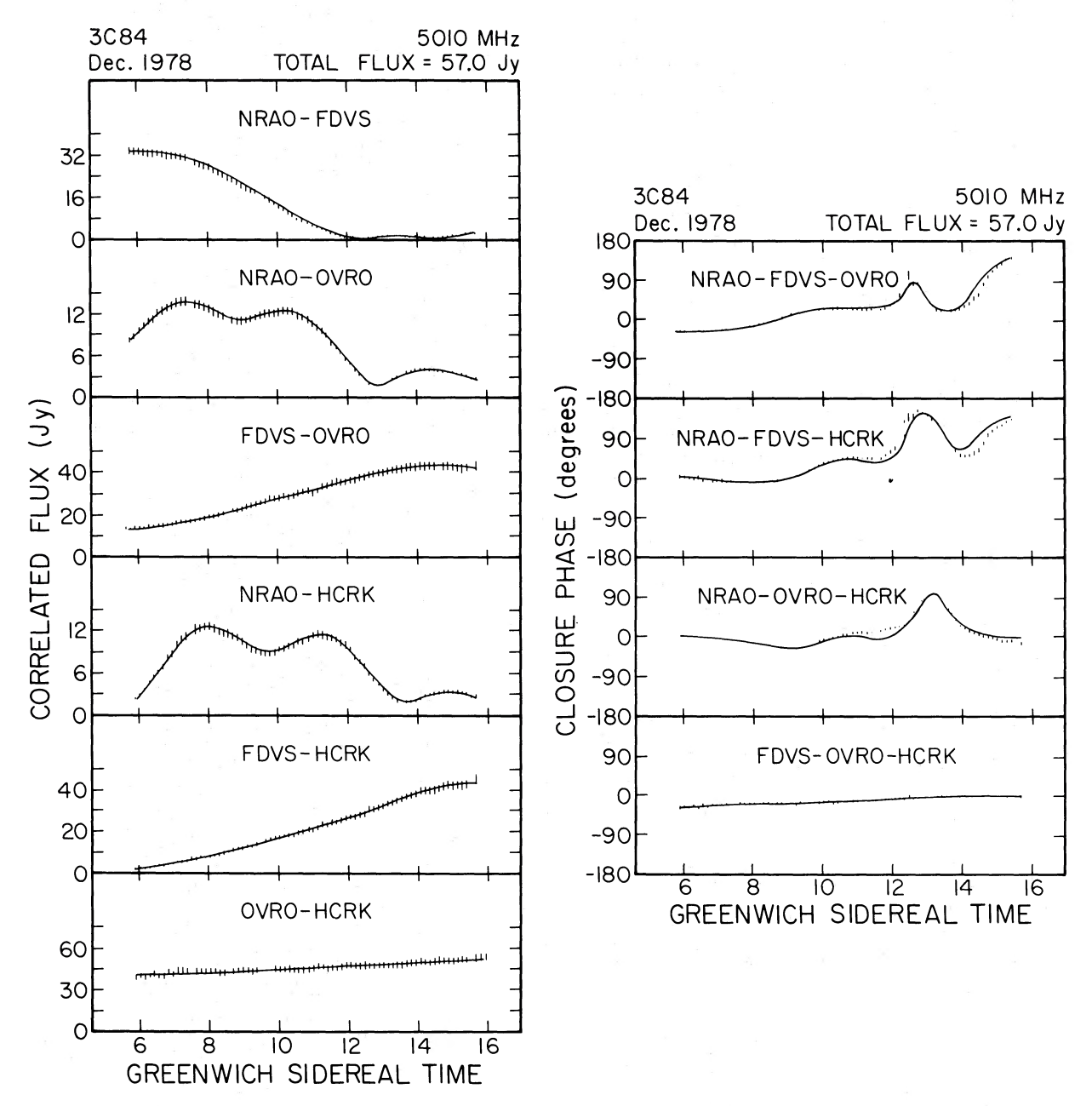


Fig. 9.—Visibility amplitudes and closure phases for 3C 84 (0316+413). The model is the hybrid map (Fig. 2).

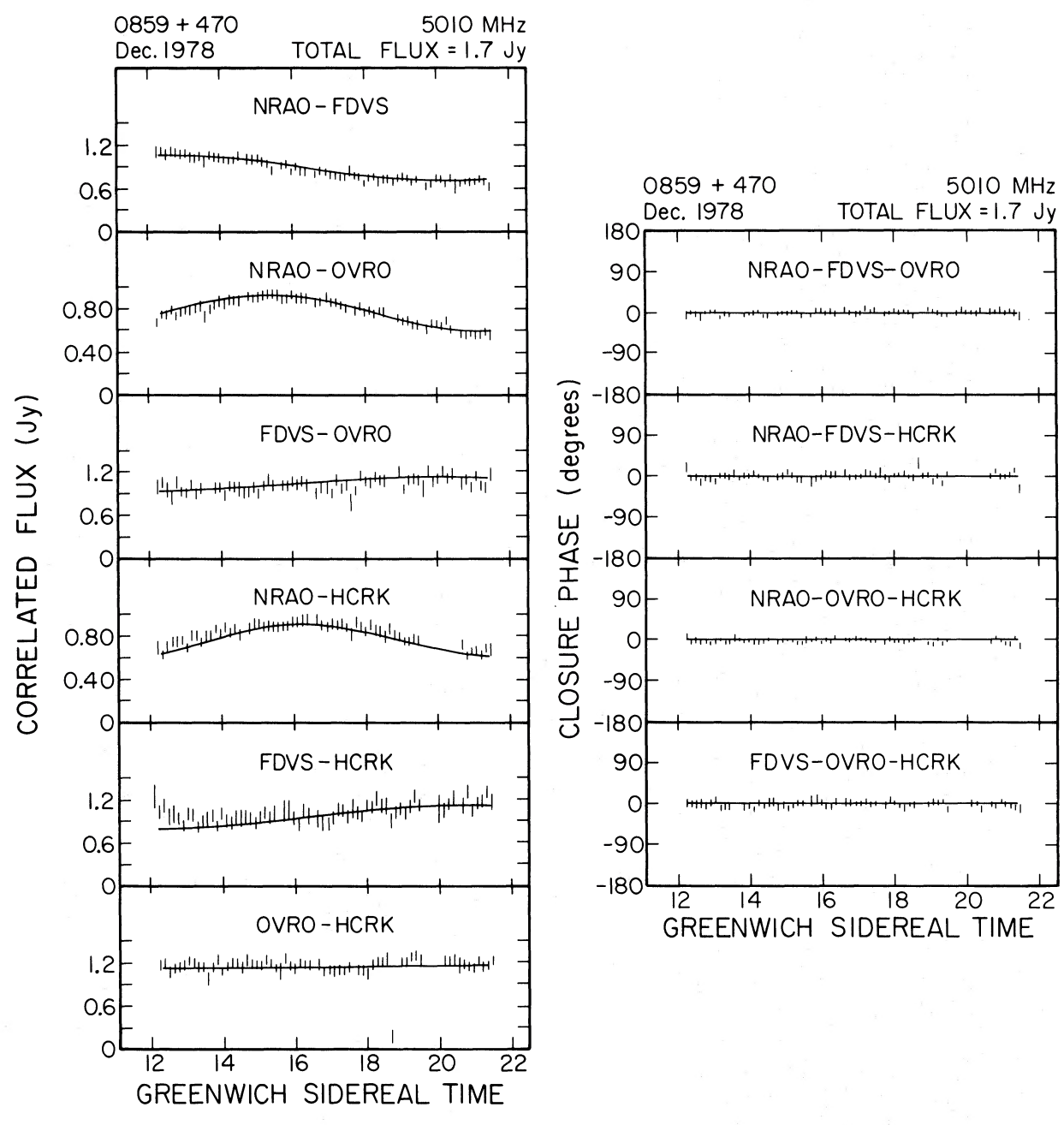


FIG. 10.—Visibility amplitudes and closure phases for 0859+470. The model is an elliptical Gaussian (Table 5).

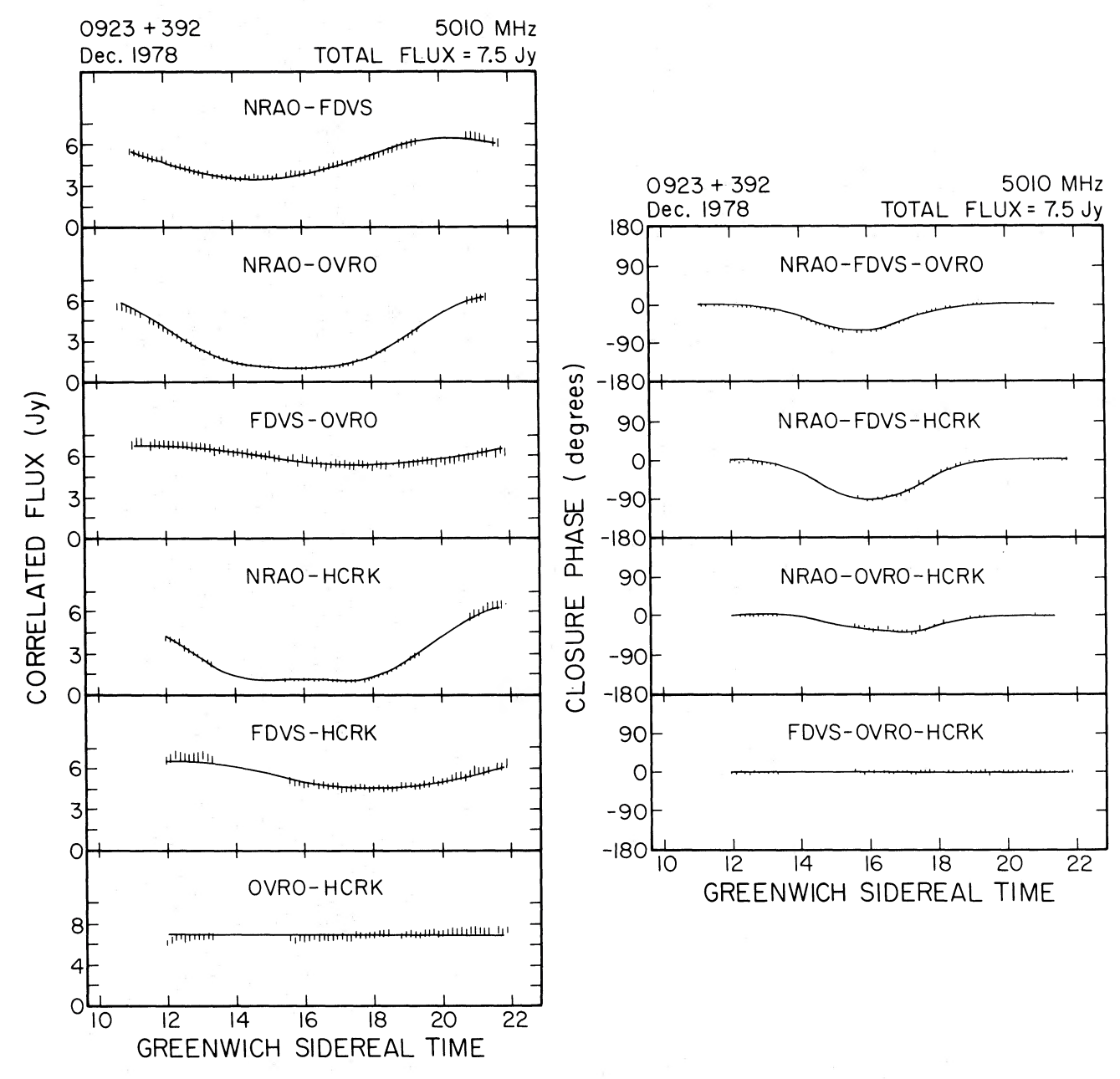


Fig. 11.—Visibility amplitudes and closure phases for 0923+392. The model consists of two circular Gaussian components (Table 5).

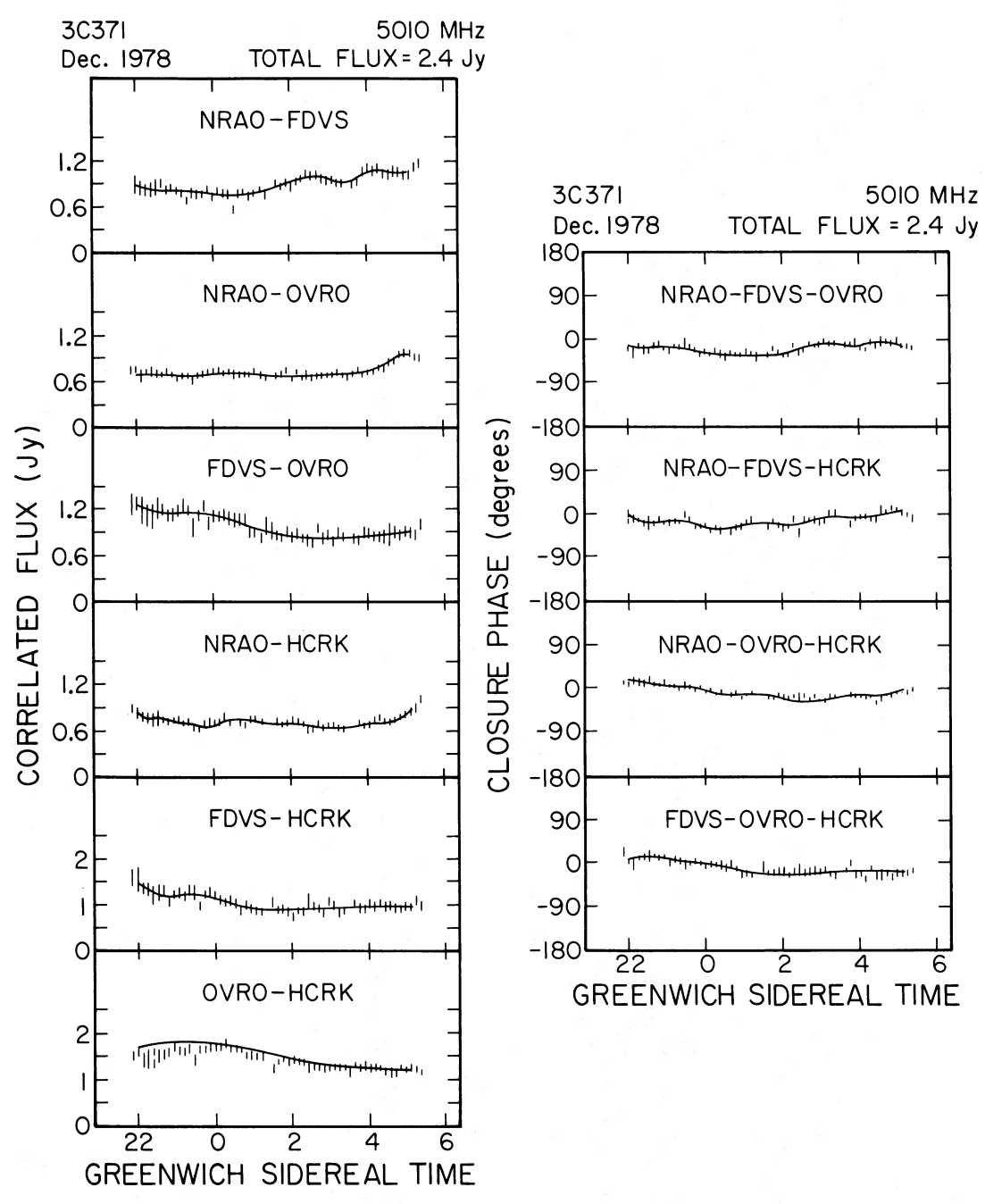


Fig. 12.—Visibility amplitudes and closure phases for 3C 371 (1807+698). The model is the hybrid map (Fig. 3).

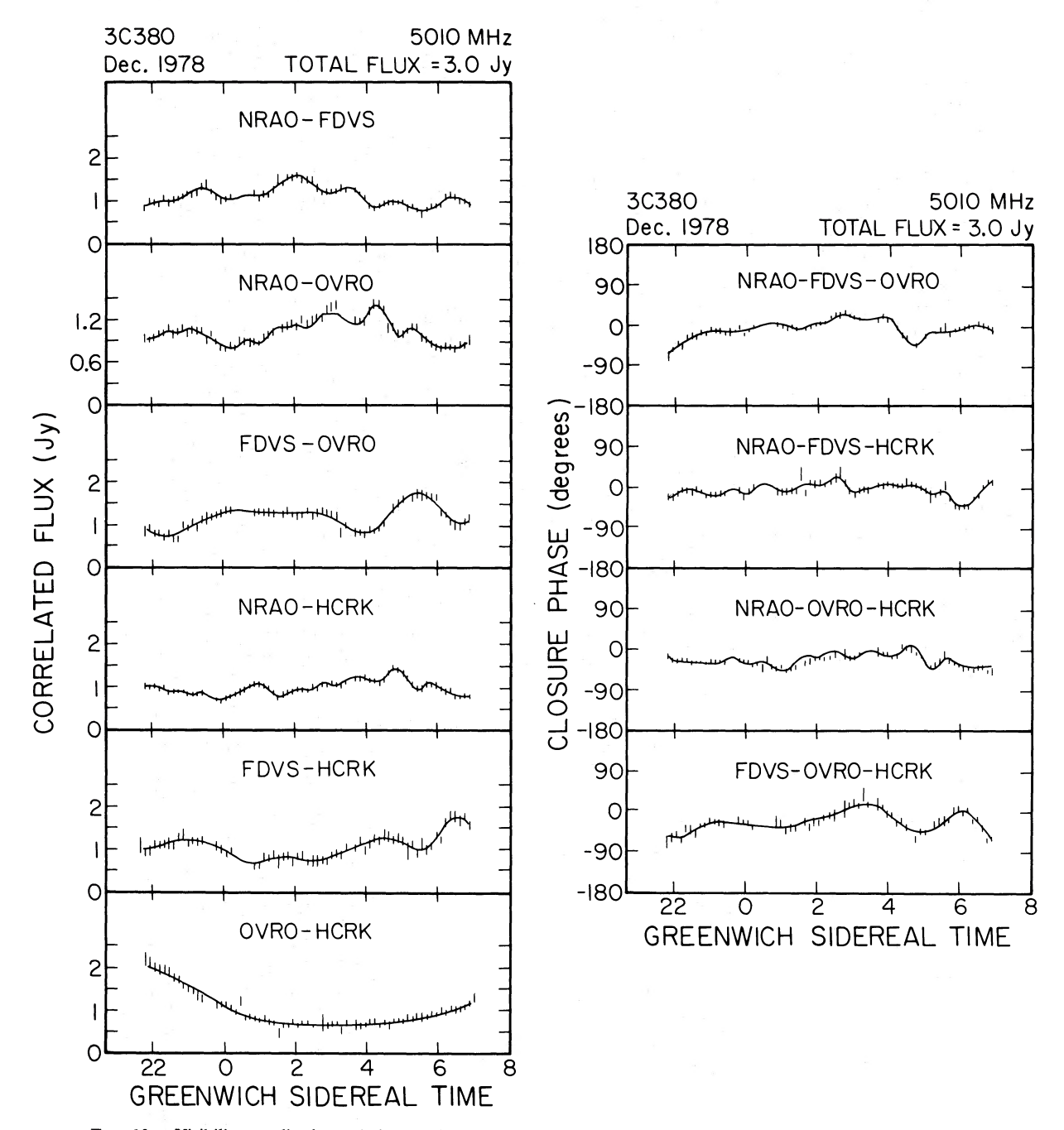


Fig. 13.—Visibility amplitudes and closure phases for 3C 380 (1828+487). The model is the hybrid map (Fig. 4).

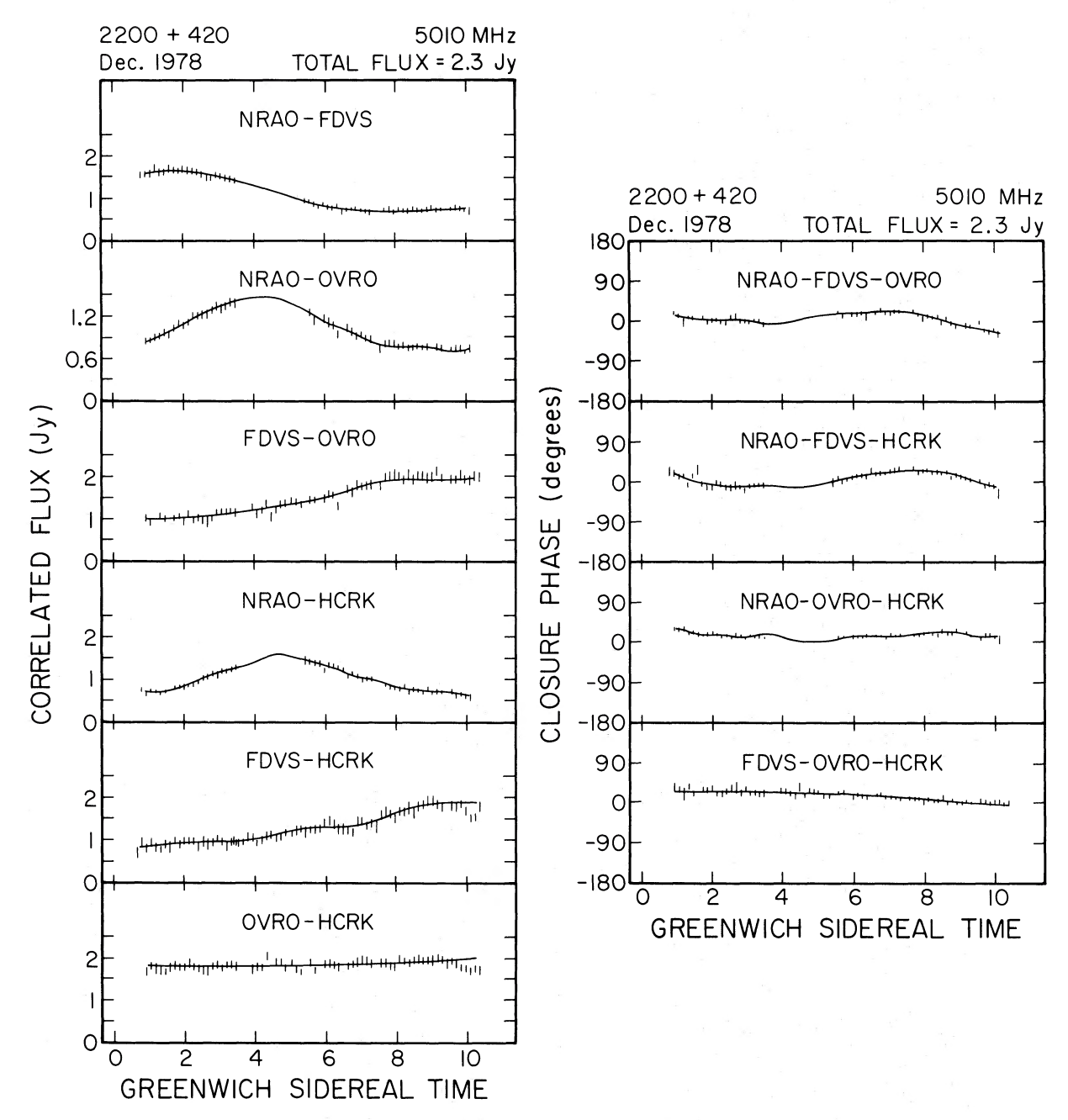


Fig. 14.—Visibility amplitudes and closure phases for BL Lac (2200+420). The model is the hybrid map (Fig. 6).

VLBI MAPS 81

REFERENCES

Andrew, B. H., Macleod, J. M., Harvey, G. A., and Medd, W. J. 1978, A.J., **83**, 863. Bååth, L. B., et al. 1980, Astr. Ap., **86**, 364. Bååth, L. B., Elgered, G., Lundqvist, G., Graham, D., Weiler, K. W., Seielstad, G. A., Tallqvist, S., and Schilizzi, R. T. 1981, K. W., Seielstad, G. A., Tallqvist, S., and Schilizzi, R. T. 1981, Astr. Ap., 96, 316.

Blandford, R. D., and Königl, A. 1979, Ap. J., 232, 34.

Burbidge, G. R., and Crowne, A. H. 1979, Ap. J. Suppl., 40, 583.

Burch, S. F. 1979, M.N. R.A.S., 186, 293.

Clark, B. G. 1973, Proc. IEEE, 61, 1242.

Cohen, A. M., Porcas, R. W., Browne, I. W. A., Daintree, E. J., and Walsh, D. 1977, Mem. R.A.S., 84, 1.

Cohen, M. H., et al. 1975, Ap. J., 201, 249.

Cohen, M. H., et al. 1977, Nature, 268, 405.

Cohen, M. H., Pearson, T. J., Readhead, A. C. S., Seielstad, G. A., Simon, R. S., and Walker, R. C. 1979, Ap. J., 231, 293.

Cohen, M. H., and Readhead, A. C. S. 1979, Ap. J. (Letters), 233, L101. Cohen, M. H., Unwin, S. C., Simon, R. S., Seielstad, G. A., Pearson, T. J., Linfield, R. P., and Walker, R. C. 1981, Ap. J., Cotton, W. D. 1979, A.J., **84**, 1122. Elsmore, B., and Ryle, M. 1976, M.N.R.A.S., **174**, 411. Fanaroff, B. L., and Riley, J. M. 1974, M.N.R.A.S., **167**, 31P. Fomalont, E. B., Miley, G. K., and Bridle, A. H. 1979, Astr. Ap., Geldzahler, B. J., Kellermann, K. I., Shaffer, D. B., and Clark, B. G. 1977, Ap. J. (Letters), 215, L5.
Hewitt, A., and Burbidge, G. R. 1980, Ap. J. Suppl., 43, 57.
Jennison, R. C. 1958, M.N.R.A.S., 118, 276. Jenkins, C. J., Pooley, G. G., and Riley, J. M. 1977, Mem. R.A.S., S4, 61.
Johnson, K. H. 1974, A.J., 79, 1006.
Kellermann, K. I., et al. 1977, Ap. J., 211, 658.
Kent, S. M., and Sargent, W. L. W. 1979, Ap. J., 230, 667.
Kühr, H., Pauliny-Toth, I. I. K., Witzel, A., and Schmidt, J. 1981, 1981, A.J., in press.
Laing, R. A. 1981a, M.N.R.A.S., 194, 301.

. 1981b, M.N.R.A.S., 195, 261.
Linfield, R. P. 1981, Ap. J., 244, 436.
Marscher, A. P. 1977, Ap. J., 216, 244. Marscher, A. P., and Shaffer, D. B. 1980, A.J., 85, 668. Matveenko, L. I., et al. 1980, Pis'ma Astr. Zh., 6, 77 (English transl. Soviet Astr. Letters, 6, 42). Medd, W. J., Andrew, B. H., Harvey, G. A., and Locke, J. L. 1972, Mem. R.A.S., 77, 109.

Miley, G. K. 1971, M.N.R.A.S., 152, 477.

Miller, J. S. 1975, Ap. J. (Letters), 200, L55.

Miller, J. S., French, H. B., and Hawley, S. A. 1978, in Pittsburgh Conference on BL Lac Objects, ed. A. M. Wolfe (Pittsburgh: University of Pittsburgh), 2, 176. University of Pittsburgh), p. 176. Minkowski, R. 1957, in IAU Symposium 4, Radio Astronomy, ed. H. C. van de Hulst (Cambridge: Cambridge University Press), p. Northover, K. J. E. 1973, M. N. R. A. S., 165, 369. Owen, F. N., Burns, J. O., and Rudnick, L. 1978, Ap. J. (Letters), Owen, F. N., Spangler, S. R., and Cotton, W. D. 1980, A.J., 85,

Pauliny-Toth, I. I. K., et al. 1976, Nature, 259, 17.
Pauliny-Toth, I. I. K., Witzel, A., Preuss, E., Kühr, H., Kellermann, K. I., Fomalont, E. B. and Davis, M. M. 1978a, A.J., 83, 451 Pauliny-Toth, I. I. K., et al. 1978b, Pis'ma Astr. Zh., 4, 64 (English transl. Soviet Astr. Letters, 4, 32).

Peacock, J. A., and Wall, J. V. 1981, M.N.R.A.S., 194, 331.

Pearson, T. J., Readhead, A. C. S., and Wilkinson, P. N. 1980, Ap. Pearson, 1. 3., Academic J., 236, 714.

Perley, R. A., Bridle, A. H., Willis, A. G., and Fomalont, E. B. 1980, A.J., 85, 499.

P. A. Fomalont, E. B., and Johnston, K. J. 1980, A.J., 85, 649.

Perley, R. A., and Johnston, K. J. 1979, A.J., 84, 1247.

Perley, R. A., Willis, A. G., and Scott, J. S. 1979, Nature, 281, 437.

Pooley, G. G., and Henbest, S. N. 1974, M.N.R.A.S., 169, 477.

Preuss, E., Pauliny-Toth, I. I. K., Witzel, A., Kellermann, K. I., and Shaffer, D. B. 1977, Astr. Ap., 54, 297.

Preuss, E., Kellermann, K. I., Pauliny-Toth, I. I. K., Witzel, A., and Shaffer, D. B. 1979, Astr. Ap., 79, 268.

Readhead, A. C. S. 1980, in IAU Symposium 92, Objects of High Redshift, ed. G. O. Abell and P. J. E. Peebles (Dordrecht-Holland: D. Reidel), p. 165. 649 L105.
Shaffer, D. B., et al. 1977, Ap. J., 218, 353.
Simon, R. S., Readhead, A. C. S., Moffet, A. T., Wilkinson, P. N., and Anderson, B. 1980, Ap. J., 236, 707.
Strittmatter, P. A., Carswell, R. F., Gilbert, G., and Burbidge, E. M. 1974, Ap. J., 190, 509.
van Breugel, W. J. M., Schilizzi, R. T., Hummel, E., and Kapahi, V. K. 1981, Astr. Ap., in press.
Walsh, D., Wills, B. J., and Wills, D. 1979, M.N.R.A.S., 189, 667.
Weiler, K. W., and Johnston, K. J. 1980, M.N.R.A.S., 190, 269.
Wilkinson, P. N., Readhead, A. C. S., Anderson, B., and Purcell, G. H. 1979, Ap. J., 232, 365.
Wilkinson, P. N., Readhead, A. C. S., Purcell, G. H., and Anderson, B. 1977, Nature, 269, 764.
Wilkinson, P. N., Readhead, A. C. S., Napier, P. J., and Bignell, C. 1981, in preparation. 1981, in preparation. Wittels, J. J., et al. 1978, A.J., 83, 560.

T. J. PEARSON and A. C. S. READHEAD: California Institute of Technology, Mail Code 102-24, Pasadena CA 91125